Radio Science, Volume ???, Number , Pages 1–24,

First Observations of the New MEXART's Digital System

J. A. Gonzalez-Esparza[1], J.C. Mejia-Ambriz[1,2], E. Aguilar-Rodriguez[1], P. Villanueva[1], E. Andrade[1], A. Magro[3], R. Chiello[4], D. Cutajar[3], J. Borg[3], and K. Zarb-Adami[3,4]

Corresponding author: J.A. González-Esparza, LANCE, Instituto de Geofísica, Unidad Michoacán, Universidad Nacional Autónoma de México, Morelia, Michoacán, México. CP 58190. (americo@igeofisica.unam.mx)

[1]LANCE, Instituto de Geofísica, Unidad Michoacán, Universidad Nacional Autónoma de México, Morelia, Michoacán, México. CP 58190.

[2]CONACyT Research Fellow – Instituto de Geofísica, Unidad Michoacán, Universidad Nacional Autónoma de México, Morelia, Michoacán, México. CP 58190.

[3]Institute of Space Sciences and Astronomy, University of Malta, Malta.

Abstract: The Mexican Array Radio Telescope (MEXART) is a transit instrument mainly dedicated to performing Interplanetary Scintillation (IPS) observations with a central operating frequency of 139.65 MHz. The main scientific objective is to perform studies of solar wind properties and space weather effects. MEXART initially operated with an analog beam former (16x16 Butler matrix), which produced 16 fixed latitudinal beams. MEXART began operations and reported the first measurements of IPS sources. MEXART's beam forming system had several problems, however. The North-South beams had poor directivity, with large side lobes, and the instrument did not achieve the expected performance. Therefore, we commissioned the design and construction of a digital back-end. The digital system solved the problems with the beam forming, increases the bandwidth, and significantly improves the instrument's sensitivity. In this paper, we present the first light of MEXART's digital system. We describe the new technical capabilities of the instrument, and we show some preliminary results: an estimation of the radio telescope's sensitivity ($\Delta S_{min} = 2.28 \pm 0.23$ Jy), the transit of the Galaxy at 140 MHz with the simultaneous tracking of 62 latitudinal beams, and an example of an IPS observation and the single-station methodology for calculating the solar wind speed. The new technical capabilities of the radio telescope will provide the potential for participating in several scientific studies. These include solar wind properties, space weather fore-

[4]Department of Astrophysics, University

of Oxford, UK

casting, ionospheric perturbations, and astrophysical aims such as the monitoring of repeating Fast Radio Bursts (FRBs) and pulsars' observations.

1. Introduction

The Mexican Array Radio Telescope (MEXART) is a transit instrument mainly dedicated to performing Interplanetary Scintillation (IPS) observations with a central operating frequency of 139.65 MHz. The site is located in Coeneo, Michoacán, Mexico (19.81° N, 101.69° W) (Figure 1). The IPS phenomenon, detected by ground-based radio telescopes, is the random flux fluctuations of a radio source when its signal is scattered by the solar wind. These fluctuations are caused by the propagation of the solar wind's electron density irregularities causing a moving diffraction pattern along the line of sight (LOS). The recording of the radio source's transit shows flux intensity fluctuations (scintillation) with a periodicity around 1s. The scintillation level in the measurements is related to the variations of the solar wind electron density along the LOS. The IPS was discovered by Margaret E. Clarke during a 178 MHz interferometric survey of radio sources in Cambridge, U.K. (Clarke, 1964). The phenomenon was analyzed and reported by Hewish, Scott, and Wills (1964). At 140 MHz, the typical limit of the angular size of the radio source for producing IPS is around 0.5" (Little & Hezmsh, 1966; Duffett-Smith, 1976).

An IPS technique to infer solar wind properties (speed and density fluctuations) is based on a power spectra analysis, where a Fast Fourier Transform is applied to the time series of the intensity fluctuations of the radio source. In general, there

is a knee in the power spectrum with a maximum around the 1 Hz regime, while the power decreases following a power law at higher frequencies. We fit the power spectrum to a physical model. This model depends on several physical parameters: solar wind speed, the apparent source size, and the power index of the wavenumber of the density irregularities (Scott et al., 1983; Manoharan & Ananthakrishnan, 1990; Mejia-Ambriz, 2012). This is known as the single-station methodology because it requires observations from only one radio telescope to calculate the solar wind speed.

To obtain reliable solar wind speed results with the single-station methodology, the observation of IPS should have a good signal-to-noise ratio, which depends on the radio telescope sensitivity. If the instrument cannot provide adequate IPS observations, the solar wind speed results of the fitting model would have, in general, larger errors (Chang et al., 2019).

MEXART's antenna is an array of 4096 full-wavelength dipoles ordered in a 64x64 element formation. The dipoles are arranged along 64 East-West (E-W) lines, covering a physical area of 8,401 m^2 (136.16 m (E-W) x 61.70 m (North-South N-S)). MEXART was originally operating with a 16x16 Butler matrix, which produced 16 fixed latitudinal beams (Gonzalez-Esparza et al., 2004). Using 1/4 of the antenna (16 E-W lines), MEXART undertook operations and reported the first measurements of IPS sources (Mejia-Ambriz et al., 2010), the detection of solar wind transient events (Romero-Hernandez et al., 2015), and the systematic observations of a few IPS sources to infer the yearly variation of their scintillation indexes (Chang et al., 2016). To improve the single-station fitting analysis, Aguilar-Rodriguez et al. (2014)

presented a new technique based on the wavelet transform for analyzing MEXART IPS data.

MEXART's original system was based on analog technology. Figure 2 shows the block diagram of the signals, from the dipoles to the beam former (Butler matrix). The signals detected by an E-W line of 64 dipoles are subdivided and collected in transmission lines into four sections of 16 dipoles each. The signal from each section passes through a high-pass filter, a first amplification step, and is combined 2:1 with the signal of the subsequent section. This resulting signal goes to a second combination level 2:1 at the middle of the line and a second amplification step, obtaining a final signal for the E-W line. The antenna with 64 E-W lines provides 64 inputs to the control room for beam forming and processing. The 16x16 Butler matrix was designed by engineers from the National Centre for Radio Astrophysics - Tata Institute of Fundamental Research in India, and it was assembled by the MEXART's team (Gonzalez-Esparza et al., 2004).

The Butler matrix is a beam former system, a network to control the phase and amplitude of RF power passing. In MEXART's analog configuration, the 16x16 Butler Matrix was located between the antenna arrays and the receiver to shape the relative spatial sensitivity of the system to RF signals originated in its field of view (Figure 2). The radiation pattern produced 16 fixed latitudinal (N-S) beams. For the six central latitudinal beams around the zenith of the instrument, their angular widths were about 1° along the E-W direction and 9° along the N-S direction. The

other lateral latitudinal beams had wider angular widths along the N-S direction (Villanueva-Hernandez, 2008).

Even though with MEXART's observations we could detect a few IPS sources to infer some solar wind's properties, the analog beam forming system presented several problems and limitations. The restriction of 16 input ports at the Butler matrix obligated us to further combine the antenna signals at the back-end to allow us to observe with half of the array (2:1 with 32 E-W lines) or the full array (4:1 with 64 E-W lines). This extra combination of the line signals produced larger errors (in phase and amplitude) for the signals injected into the Butler matrix that affected the beam-formation. We tried several techniques to solve these issues, but our compensation solutions were only temporary. The 16 N-S beams produced by the Butler matrix had poor directivity (with very large N-S side lobes), which caused significant gain losses, and the instrument did not approach the expected response. These technical problems prevented the radio telescope from detecting the number of radio sources required to monitor the solar wind between the Sun and the Earth. Furthermore, the IPS observations did not have a good signal-to-noise ratio for most of the radio sources, which is required by the single-station technique to obtain reliable solar wind parameters. We needed to upgrade the back-end system to reach the expected performance.

In 2014, the Mexican Space Weather Service was established to monitor and alert decision-makers about space weather conditions that compromise critical technologies in Mexico (Gonzalez-Esparza et al., 2017). Although space-based coronagraphs

can detect the expulsion of coronal mass ejections in the solar atmosphere, their field of view is limited to a few dozen solar radii. A very fast and hypothetical geoeffective coronal mass ejection, propagating towards the Earth, could travel several hours without ground tracking until it reaches the L1 position, where a spacecraft would take in-situ measurements and finally providing an early warning of only a few minutes. The IPS observations may be used as a remote sensing technique to measure solar wind disturbances, which can potentially detect solar wind's large-scale perturbations for some hours (up to days) in advance before they reach 1 AU (Romero-Hernandez et al., 2015). The necessity of monitoring space weather conditions, as well as to accomplishing the aims of scientific studies, led us to improve the detection of IPS radio sources and, hence to upgrade MEXART's analog back-end to a digital system.

This paper introduces the first light of MEXART's digital system. The outline of the paper is as follows: Section 2 describes the new technical capabilities of the digital instrument and compares them with the previous analog configuration. Section 3 shows some preliminary results: an estimation of the instrument's sensitivity, the observation of the transit of the Galaxy at 140 MHz, and an IPS observation where we used the single-station methodology to infer the solar wind speed. Section 4 comments on other possible scientific applications for the new radio telescope's capabilities, and Section 5 presents a summary.

2. MEXART digital upgrade: system specifications

Based on the necessity of improving the response of the radio-telescope, we upgraded the analog back-end to a digital system. The description of the digital upgrade is described in detail elsewhere (Magro et al., 2019; Magro et al., 2021). Figure 3 shows a block diagram of the digital back-end. The signals of the 64 E-W lines from the antenna travel through three levels of amplification, after which they are connected to the two FPGA boards. The RF-conditioned analogue signals are transported to the RF inputs of two Tile Processing Modules (TPMs) (Naldi et al., 2018), which are custom FPGA boards developed for the Square Kilometre Array (SKA), hosting 8 dual AD9680 Analog to Digital Converter (ADCs) and two Xilinx Kintex Ultrascale XCKU040 FPGAs. The signals are down-converted, digitized, and channelized into 2048 frequency channels using a polyphase filter bank channelizer, 512 of which are chosen for further processing and represent the central 12.5 MHz frequency band of MEXART. These frequency channels are packetized and transmitted over a 40Gb Ethernet connection to a processing server, which captures the packets and beam-forms or correlates the data. The beamformer and correlator are custom CUDA implementations that run on an NVidia Tesla P40. During normal operation, the beamformer generates up to 64 independent, integrated and calibrated synthesized N-S beams within the array's primary Field of View in real time, the integration time for which is configurable. The shape of each synthesized beam depends on the pointing as shown in Figure 6. To compensate for instrumental delays which de-

cohere the signals, a calibration observation is routinely performed using a custom GPU-based correlator that calculates the correlation matrix for the array.

Figure 4 shows the 64 antenna signals arriving at the control room and connecting to the two FPGA boards. The software can analyze the amplitude and phase of the 64 input digitalized signals. The system runs calibration observations to obtain correlation coefficients that compensate digitally (in phase and amplitude) the 64 signals from the antennas. As commented on above, by running a calibration observation on a routine basis, we corroborate the stability of the system. Typically, calibration observations are performed on strong astronomical sources when they are at their highest altitude. The observation starts 5 m before peak transit time and runs for 10 m. During this time, the 64 channelized antenna signals are cross-correlated and integrated to generate a correlation matrix every 1 s. Once the observation is complete the calibration procedure is applied. First, the peak transit time within the observation is calculated, and the corresponding correlation matrix, as well as the ones 10 s before and after that time, are selected. For each matrix, a StEFCal calibration is performed (Salvini & Wijnholds, 2014), generating the calibration coefficients. The best coefficient set out of the three is chosen and saved to a database. Subsequent beam forming observations then use the updated calibration coefficients.

Table 1 summarizes some technical capabilities of the digital system and compares them with the analog configuration. The digital system, based on two FPGA boards and software, has new capabilities in beam forming, bandwidth, and frequency resolution. The digital system has a wider bandwidth of 12.5 MHz, covering

a frequency range from 133.4 to 145.9 MHz, with a frequency resolution of 24.4 KHz (512 channels). Another advantage is that now the instrument can detect with a higher sampling rate (1 ms). The digital system produced significant improvements in directivity and sensitivity, reaching the expected performance.

3. Preliminary results

3.1. Estimation of the array's sensitivity

The normalized one-dimensional beam pattern, P, (for a rectangular array of aperture l and observing wavelength λ) can be modeled as a function of the angular direction θ in the sky by

$$P(\theta) = \left(\frac{\sin(\Theta)}{\Theta}\right)^2, \tag{1}$$

with $\Theta = \frac{\pi l}{\lambda}\sin(\theta)$. Figure 5 shows (red curve) MEXART's theoretical beam pattern along the E-W direction (l_x = 136.16 m, λ=2.14 m). The pattern is proportional to the received signal power and to the output voltage $V = rP$, where r is the responsivity. The full width at half maximum (FWHM) of the beam, according to a one-dimensional aperture, is $0.89\,\lambda/l_x$ radians or 0.80° (Marr et al., 2015), which corresponds to the width of the beam along the E-W direction. Similarly, the beam along the N-S direction ($l_y = 61.7$ m) is 1.77°.

Because of MEXART's geographic location (19.81° N), it is convenient to use 3C144 (SNR Crab Nebula) measurements to infer the antenna beam pattern and to estimate the instrument's sensitivity in total power mode. The radio flux of 3C144 is very well studied and has a flux density of 1395 Jy at 140 MHz (Perley & Butler, 2017). This

radio source can be considered as a point source by MEXART's beams, and its transit is close to the local zenith. Figure 5 shows a transit of 3C144 observed by MEXART (black curve) compared with the expected beam pattern along the E-W direction (red curve). For this observation, we used the synthesized beam configuration to point the beam in total power mode towards the radio source. By analyzing 17 transits of 3C144 detected with the synthesized beam, we got a FWHM average of 0.86 with a standard deviation of 0.06 degrees. Comparing this average to the expected value of 0.80 degrees, the resulting percent error in the FWHM average is 7%. As is shown in Figure 5, the theoretical radiation pattern has a very good fit with the observations. The amplitude and direction of the side lobes also agree very well. As expected, the first side lobes are very close to 5% of the level of the main lobe.

With these observations, we can estimate the instrument's sensitivity. The beam's solid angle through all the power Ω_A is related to the effective antenna aperture A_e as

$$A_e = \frac{\lambda^2}{\Omega_A}. \tag{2}$$

For a two-dimensional array with beamwidths that are θ_x and θ_y, $\Omega_A = 1.33\,\theta_x\,\theta_y$ (Kraus, 1986). By assuming that the beam is about 7% wider along the N-S direction (1.89°), $A_e = 6954\,\mathrm{m}^2$. Therefore, an antenna efficiency of $\eta = 0.82$ can be assumed, with a gain of 42.9 dB in total power mode.

By analyzing 15 transits of 3C144 during February 2021 (using the full bandwidth $\Delta\nu = 12.5$ MHz and a sampling time $\tau = 20$ ms), the minimum detectable flux density is $\Delta S_{min} = 1395\,\mathrm{Jy/N}_\sigma$, where N_σ is the observed intensity normalized to

sigma noise ($N_\sigma = I/\sigma_I$ units). From this, we get a minimum detectable flux $\Delta S_{min} = 2.28 \pm 0.23$ Jy.

By using ΔS_{min} we can estimate the temperature of the system T_s by

$$T_s = \frac{A_e\sqrt{\Delta\nu\,\tau}}{2\,K_B}\Delta S_{min}, \tag{3}$$

with K_B as the Boltzmann constant and K_r as the sensitivity constant. Table 2 shows the resulting ΔS_{min}, T_s and the sigma noise temperature of the system (ΔT) for three different bandwidths of the spectrometer.

The resulting $T_s = 2872$ K is higher than the value reported for the analog configuration with a shorter bandwidth ($T_s = 475$ K (Mejia-Ambriz et al., 2010)). This higher value in the system's temperature might be due to the filtering effect in the bandwidth added to the digital configuration, which attenuates the sensitivity at the two extremes of the bandwidth. MEXART's digital system has a sensitivity's peak of around $\sim 135 - 142$ MHz, and the rest of the bandwidth tends to have lower sensitivities.

For an ideal case (having maximum sensitivity across the entire bandwidth), we can use the best 24.4 KHz channel to calculate Ts. Employing Equation 3, we obtain $T_s = 1280$ K. For this ideal case, with all channels responding with the same best sensitivity, ΔS_{min} would be < 1 Jy. By subtracting the value of 295 K of the sky temperature at 140 MHz (McKinley et al., 2012), the temperature of the instrument would be 985 K.

3.2. Mapping observations of 140 MHz radio sky

One of the limitations of the former analog system was the poor directivity of the 16 latitudinal N-S beams produced by the Butler matrix. The N-S beam pattern had latitudinal side lobes with significant high gains, and the power of the secondary beams was comparable with the main beams. This directivity issue prevented the possibility of mapping the radio sky with the 16 latitudinal beams. As previously mentioned, the digital system allows different configurations of latitudinal beams. Figure 6 shows MEXART's digital configuration of 62 fixed simultaneous latitudinal N-S beams. The 62 beams point at different well-defined declinations, and their signals are recorded by the digital back-end. Using this configuration, along with the Earth's rotation, it is possible to measure the flux of the transit of the Galaxy during a single day. Figure 7 shows an observation of the transit of the Galaxy at 139.65 MHz detected by MEXART on April 10th, 2021. We used an integration time of 1.5 s for this observation. The plot shows the integrated flux density (512 frequency channels) as detected by the 62 latitudinal beams versus sidereal time. Each beam tracks a latitudinal band across the radio sky. The comparison of the 62 records shows the transit of the Galaxy at different declinations. The shapes of the Galaxy's nucleus and arm appear clearly in the combined curves. The Sun is the strongest radio source in the sky, which transited at 1:20 ST, 3C405 (Cygnus A) at 19:59 ST, 3C461 (Cassiopeia A) at 23:23 ST, and 3C144 (Crab Nebula) at 5:34 ST.

Figure 8 shows the contours of the transit of the Galaxy at 139.65 MHz using the measurements of the 62 fixed declination beams. This is the same observation as in Figure 7, but in this case we removed the interferences and applied a numerical

filter to smooth the gradients. We overplot contour curves to emphasize the radio flux zones in the Galaxy. The plot shows the transit of the strong sources commented on in Figure 7. This observation clearly shows that the 62 latitudinal beams' configuration possess good directivity, and now the radio telescope can track the radio sky.

3.3. IPS observations

The main aim of MEXART's upgrade is to improve the response in detecting IPS sources. Figure 9(a) shows the record of the radio source 3C48 (J0137 + 331) obtained by the MEXART on April 8, 2021. The new digital back-end can produce a synthesized beam towards a required declination. For this observation, we employed this configuration that will be used for our IPS surveys in the future. The temporal resolution of the data is 20 ms (50 intensity data points per second). Each data point corresponds to the integrated flux by adding the 512 frequency channels at normalized intensity. Figure 9(a) shows the IPS characteristic signature of good level of scintillation in a time window of about four minutes (19:14-19:18 UT). There is also a strong interference around 19:20, which is associated with an emission from a satellite.

Previous studies have shown that the wavelet transform (WT) can be used in the analysis of IPS observations (Aguilar-Rodriguez et al., 2014; Romero-Hernandez et al., 2015). Figure 9(b) shows the WT power spectrum after applying the WT to the time series of Figure 9(a) using the code of Torrence and Compo (1998). In order to apply the WT, we previously removed possible contributions caused by ionospheric scintillation in the data by subtracting the running mean of 10 s, which equals 500

data points in the time series. Figure 9(b) shows that the WT power spectrum during the IPS signature appears with predominantly red tones, and it coincides with the time window of the time series in Figure 9(a). There is also the signature of the interference caused by a satellite emission. From the WT, we can obtain the power spectrum of the signal. This is done by obtaining the average power in each and every frequency channel of the portion of the WT power spectrum delimited by the dashed-line box shown in Figure 9(b). The frequency range that the dashed-line box covers ranges from 0.1 Hz up to 10 Hz. This allows the power spectrum to be constructed like the one shown in Figure 9(c). Aguilar-Rodriguez et al. (2015) present a comparison of the power spectra obtained with both the WT and Fourier analyses. The results show that the two power spectra are similar, however, the power spectra obtained with the WT analysis turned out to be slightly cleaner and with a greater level of intensity of fluctuations (13 % greater than the one using the Fourier analysis). For this reason, we chose the WT technique to analyze MEXART IPS data.

Once the observed power spectrum of the 3C48 radio source has been obtained, we perform the speed calculation using the single-station analysis methodology (Manoharan & Ananthakrishnan, 1990). We followed the methodology used in a previous analysis (Mejia-Ambriz et al., 2015; Chang et al., 2016, 2019). Figure 10 shows the fit of the theoretical spectrum with the observed one. For this case, we assume the existence of an isotropic solar wind and that there are no contributions from the inner scale. We used values reported previously in the literature (the axial

ratio (AR) of the solar wind irregularities=1.0 and the power-law index of density turbulence spectrum α=3.5 (Mejia-Ambriz et al., 2015)), to fit the solar wind speed. The estimated error is given by χ^2. The solar wind speed turns out to be 809 km/s, which corresponds to a fast solar wind stream. The spectral fitting is shown up to 10 dB to highlight the Fresnel knee region, which is around 1 Hz, because it is the most involved with the solar wind speed.

Figure 11(a), shows an image of the Sun observed on April 8, 2021 by the Atmospheric Imaging Assembly (AIA) onboard the Solar Dynamics Observatory (SDO) mission. Figure 11(b) shows the apparent location of 3C48 in the sky. The 3C48's elongation was in the weak scattering region of solar wind turbulence at 140 MHz. It can be seen that the LOS of 3C48 was above the polar coronal hole that is shown in Figure 11(a). The fast solar wind obtained from the IPS analysis agrees qualitatively with the expected solar wind coming from a polar coronal hole.

4. Other applications in addition to IPS observations

The main scientific objective of the instrument is to perform daily observations of IPS sources (during the daytime). The good sensitivity and directivity of the radio telescope would allow performing routinely measurements of at least a few dozen IPS sources to provide solar wind data that can be used for space weather forecasting purposes. MEXART's observations would complement the daily IPS measurements by the ISEE antennas of the Nagoya University in Japan (Tokumaru et al., 2011), which had provided daily solar wind data for several years. The new technical ca-

pabilities from the digital upgrade allow us also to plan further observations. We present a shortlist of possible applications for other astrophysical studies. (1) Monitoring of repeating Fast Radio Bursts (FRBs), over a periods of 10 to 100s of days, requires a great deal of telescope time, and MEXART is capable of forming multiple beams to monitor several repeaters. (2) Surveying for new FRBs. (3) Observations of pulsars, we can reduce the sampling time to 5.2 μs , which is typical for pulsar observations, and we have a good number of frequency sub bandwidths. (4) Measurements of ionospheric scintillation. (5) Solar radio bursts, and (6) observations of Jupiter flares.

5. Summary

The first results presented in this paper show that the directivity problems of MEXART's beam forming analog system were completely solved with the new digital back-end. The radio telescope now has new technical capabilities that significantly improve its performance: higher sensitivity, wider bandwidth, and 512 frequency channels. The digital system can measure the gain and the phase of the 64 input signals coming from the antenna, and, by using calibration coefficients, it can compensate for the signal differences. We presented the first observations to show that two different beam configurations (a synthesized beam and 62 fixed latitudinal beams) obtained good observations with the expected beam patterns and sensitivity. Future work includes the survey of a new catalog of IPS sources, software to clean the frequency bands of interferences, the participation in international campaigns of

solar wind studies, the automation of the IPS single-station methodology to produce solar wind data for space weather forecasting, and the extension of the instrument's observations for other astrophysical studies.

Acknowledgments. We thank to the two referees for useful comments to improve the manuscript. We would like to dedicate this paper to the memory of Silvia Bravo (1945-2000), founder of the IPS project in Mexico. She would be very pleased with the new capabilities of the digital system. We are grateful to Oyuki Chang and Stan Kurtz for reading the manuscript and providing very useful comments. The MEXART's data archiving is underway. We upload a copy of the data as Supporting Information for review purposes. Data sets for this research are deposited in Zenodo: Gonzalez-Esparza, Aguilar-Rodriguez, Mejia-Ambriz, Villanueva-Hernández, and Andrade-Mascote (2021), [with the Creative Commons Attribution 4.0 International license]. LANCE acknowledges partial support from CONACyT-AEM Grant 2017-01-292684 and LN 315829. J.C. Mejia-Ambriz is grateful for the 256033 CONACyT project. E. Aguilar-Rodriguez acknowledges support from DGAPA/PAPIIT project IN103821.

References

Aguilar-Rodriguez, E., Mejia-Ambriz, J. C., Jackson, B. V., Buffington, A., Romero-Hernandez, E., Gonzalez-Esparza, J. A., ... Manoharan, P. K. (2015). Comparison of solar wind speeds using wavelet transform and fourier analysis in ips data. *Solar Physics*, *290*, 2507-2518. doi: 10.1007/s11207-015-0758-0

Aguilar-Rodriguez, E., Rodriguez-Martinez, M., Romero-Hernandez, E., Mejia-Ambriz, J. C., Gonzalez-Esparza, J. A., & Tokumaru, M. (2014). The wavelet transform function to analyze interplanetary scintillation observations. *Geophys. Res. Lett.*, *41*, 3331-3335. doi: 10.1002/2014GL060047

Chang, O., Bisi, M., Aguilar-Rodriguez, E., Fallows, R. A., Gonzalez-Esparza, J. A., Chashei, I., & Tyul'bashev, S. A. (2019). Single-site ips power spectra analysis for space weather products using cross-correlation function results from eiscat and merlin ips data. *Space Weather*, *17*, 1114-1130. doi: 10.1029/2018SW002142

Chang, O., Gonzalez-Esparza, J. A., & Mejia-Ambriz, J. C. (2016). Ips observations at 140 mhz to study solar wind speeds and density fluctuations by mexart. *Advances in Space Research*, *57*, 1307-1313.

Clarke, M. E. (1964). *Two topics in radiophysics. i. some observations of discrete radio sources. ii. an investigation of ionospheric irregularities using a radio signal from an artificial satellite* (5097). University of Cambridge.

Duffett-Smith, P. J. (1976, November). A determination of the mean angular size of scintillating radio sources at low flux densities. *Mon. Not. R. Astron. Soc.,*, *177*, 349-356. doi: 10.1093/mnras/177.2.349

Gonzalez-Esparza, J. A., Aguilar-Rodriguez, E., Mejia-Ambriz, J. C., Villanueva-Hernández, P., & Andrade-Mascote, E. (2021, June). *First observations of the new mexart's digital system (version 1.0) [data set]. zenodo.* doi: 10.5281/zenodo.4891337

Gonzalez-Esparza, J. A., Carrillo, A., Andrade, E., R., P., & Kurtz, S. (2004). The mexart interplanetary scintillation array in mexico. *Geofisica Internaciona*, *43*(1), 61-73.

Gonzalez-Esparza, J. A., De la Luz, V., Corona-Romero, P., Mejia-Ambriz, J. C., Gonzalez, L. X., Sergeeva, M. A., ... Aguilar-Rodriguez, E. (2017). Mexican space weather service (sciesmex). *Space Weather*, *15*(1), 3-11. Retrieved from `https://agupubs.onlinelibrary.wiley.com/doi/abs/10.1002/2016SW001496` doi: https://doi.org/10.1002/2016SW001496

Hewish, A., Scott, P., & Wills, D. (1964). Interplanetary scintillation of small diameter radio sources. *Nature*, *203*.

Kraus, J. D. (1986). *Radio astronomy* (2nd edition ed.). McGraw-Hill.

Little, L. T., & Hezmsh, A. (1966, 12). Interplanetary Scintillation and its Relation to the Angular Structure of Radio Sources. *Monthly Notices of the Royal Astronomical Society*, *134*(3), 221-237. Retrieved from `https://doi.org/10.1093/mnras/134.3.221` doi: 10.1093/mnras/134.3.221

Magro, A., Borg, J., Chiello, R., Cutajar, D., Zarb Adami, K., González-Esparza, J. A., ... Villanueva-Hernandez, P. (2021, September). Digitizing MEXART – System Overview and Verification. *arXiv e-prints*, arXiv:2109.11329.

Magro, A., Chiello, R., Cutajar, D., Borg, J., Zarb-Adami, K., Gonzalez-Esparza, J. A., ... Andrade-Mascote, E. (2019). A new digital backend for the mexican array radio telescope. In *2019 international conference on electromagnetics in advanced applications (iceaa).* doi: 10.1109/ICEAA.2019.8878959

Manoharan, P., & Ananthakrishnan, S. (1990). Determination of solar-wind velocities using single-station measurements of interplanetary scintillation. *Mon. Not. Roy. Astron. Soc.*, *244*, 691.

Marr, J., Snell, R., & Kurtz, S. (2015). *Fundamentals of radio astronomy: Observational methods*. CRC Press. Retrieved from https://books.google.com.mx/books?id=T54oCwAAQBAJ doi: 10.1201/b20506

McKinley, B., Briggs, F., Kaplan, D. L., Greenhill, L. J., Bernardi, G., Bowman, J. D., ... Wyithe, J. S. B. (2012, dec). LOW-FREQUENCY OBSERVATIONS OF THE MOON WITH THE MURCHISON WIDEFIELD ARRAY. *The Astronomical Journal*, *145*(1), 23. Retrieved from https://doi.org/10.1088%2F0004-6256%2F145%2F1%2F23 doi: 10.1088/0004-6256/145/1/23

Mejia-Ambriz, J. C. (2012). *Análisis de observaciones del mexart: bases para estudios de centelleo interplanetario* (Unpublished doctoral dissertation). Posgrado en Ciencias de la Tierra, Universidad Nacional Autónoma de México.

Mejia-Ambriz, J. C., Jackson, B. V., Gonzalez-Esparza, J. A., Buffington, A., Tokumaru, M., & Aguilar-Rodriguez, E. (2015, may). Remote-sensing of solar wind speeds from IPS observations at 140 and 327 MHz using MEXART and STEL. *Solar Physics*, *290*(9), 2539–2552. Retrieved from https://doi.org/10.1007%2Fs11207-015-0694-z doi: 10.1007/s11207-015-0694-z

Mejia-Ambriz, J. C., Villanueva-Hernandez, P., González-Esparza, J. A., Aguilar-Rodriguez, E., & Jeyakumar, S. (2010). Observations of interplanetary scintillation (ips) using the mexican array radio telescope (mexart). *Solar Physics*,

265(1), 309-320,. doi: 10.1007/s11207-010-9562-z

Naldi, G., Comoretto, G., Chiello, R., Pastore, S., Pupillo, G., Mattana, A., ... Adami, K. Z. (2018). Development of a new digital signal processing platform for the square kilometre array. In *2018 2nd ursi atlantic radio science meeting (at-rasc)* (p. 1-4). doi: 10.23919/URSI-AT-RASC.2018.8471592

Perley, R. A., & Butler, B. J. (2017). An accurate flux density scale from 50 MHz to 50 GHz. *The Astrophysical Journal Supplement Series*, *230*(1), 7. Retrieved from `https://doi.org/10.3847%2F1538-4365%2Faa6df9` doi: 10.3847/1538-4365/aa6df9

Romero-Hernandez, E., Gonzalez-Esparza, J. A., Aguilar-Rodriguez, E., Ontiveros-Hernandez, V., & Villanueva-Hernandez, P. (2015, may). Detection of solar wind disturbances: Mexican array radio telescope IPS observations at 140 MHz. *Solar Physics*, *290*(9), 2553–2566. Retrieved from `https://doi.org/10.1007%2Fs11207-015-0690-3` doi: 10.1007/s11207-015-0690-3

Salvini, S., & Wijnholds, S. J. (2014). Stefcal — an alternating direction implicit method for fast full polarization array calibration. In *2014 xxxith ursi general assembly and scientific symposium (ursi gass)* (p. 1-4). doi: 10.1109/URSIGASS.2014.6930038

Scott, S., Coles, W. A., & Bourgois, G. (1983). Solar wind observations near the sun using interplanetary scintillation. *Astron. Astrophys*, *123*(207).

Tokumaru, M., Kojima, M., Fujiki, K., Maruyama, K., Maruyama, Y., Ito, H., & Iju, T. (2011). A newly developed uhf radiotelescope for interplane-

tary scintillation observations: Solar wind imaging facility. *Radio Science*, *46*(5). Retrieved from https://agupubs.onlinelibrary.wiley.com/doi/abs/10.1029/2011RS004694 doi: https://doi.org/10.1029/2011RS004694

Torrence, C., & Compo, G. P. (1998). A practical guide to wavelet analysis. *Bulletin of the American Meteorological Society*, *79*(1), 61-78. doi: 10.1175/1520-0477

Villanueva-Hernandez, P. (2008). *Observaciones de fuentes de radio detectadas en el mexart con una matriz de butler de 16 x 16* (Unpublished master's thesis). Posgrado en Ciencias de la Tierra, Universidad Nacional Autónoma de México.

Figure S1. Panoramic view of the MEXART site (19.81° N, 101.69° W).

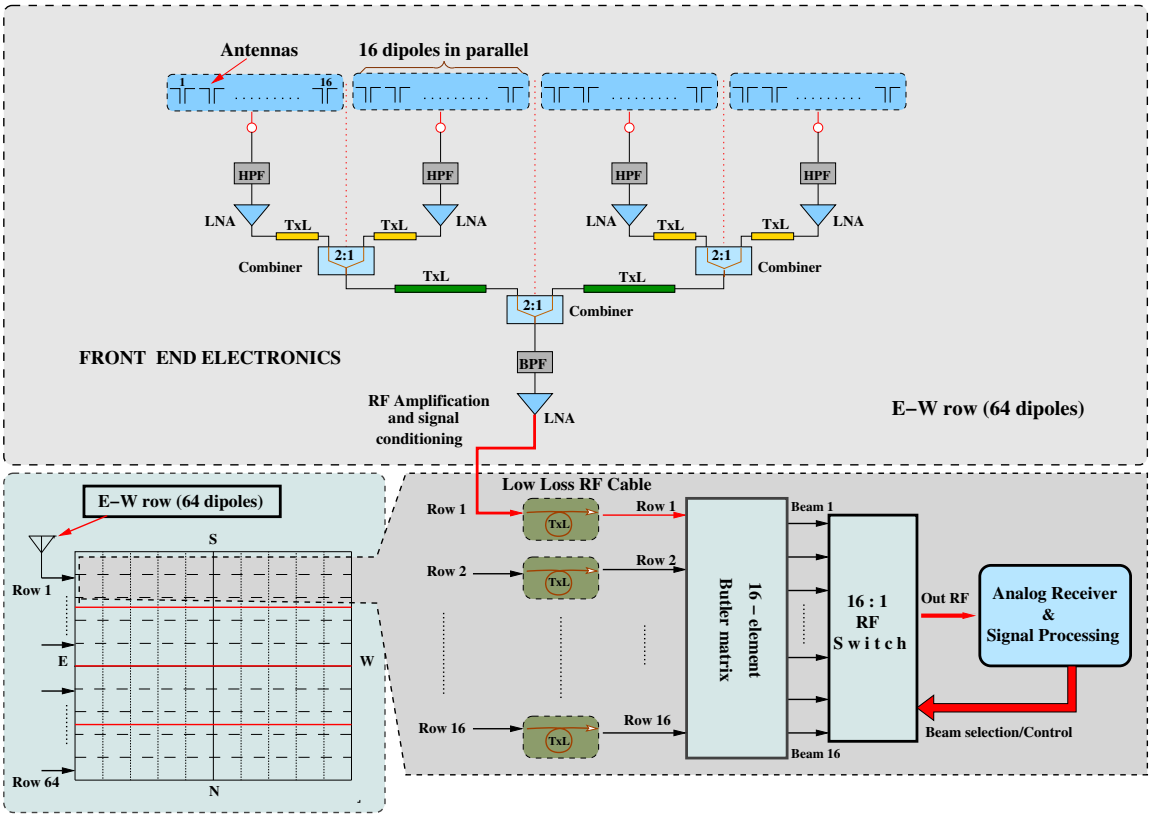

Figure S2. Block diagram of the MEXART's antenna signals processes and its original beam forming analog system (16x16 Butler matrix).

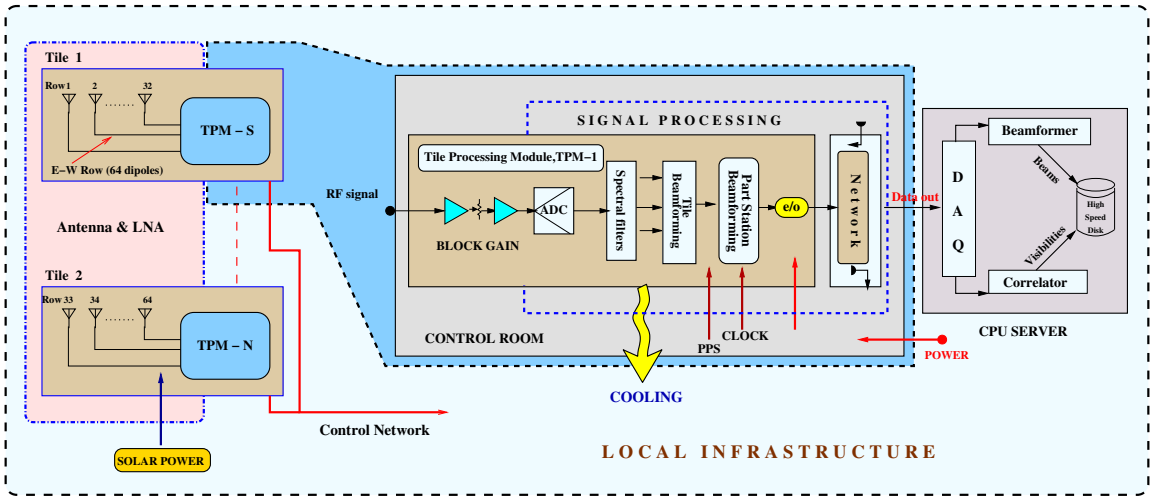

Figure S3. Block diagram of the new MEXART's digital back-end.

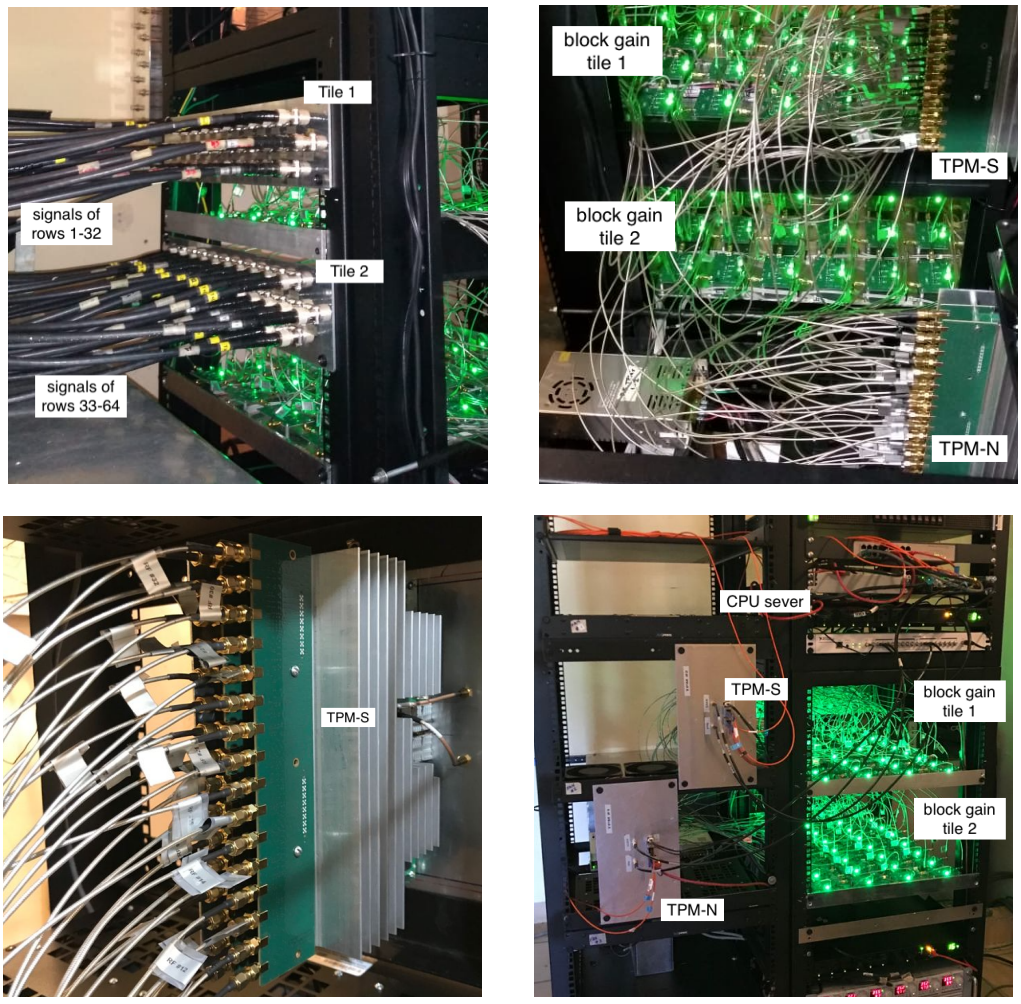

Figure S4. Pictures of the MEXART's digital back-end at the control room.

Table S1. Comparison of the characteristics of the two MEXART's configurations: analog and digital systems.

parameter	analog system	digital system
beam former	Butler matrix	FPGA firmware and software
central frequency	139.65 MHz	139.65 MHz
banwidth	1.5 MHz	12.5 MHz
frequency channels	1	512
latitudinal beams	16	several configurations
sensitivity	1/4 array $\rightarrow$ 20-30 Jy	full array $\rightarrow$ 2.3 Jy
	1/2 array $\rightarrow$ 15 Jy	
	full array $\rightarrow$ 20 Jy	
sampling rate	20 ms	40.96 bus, integration time (0.5ms-2s)
extra capabilities		real-time monitoring of the input antenna signals
		amplitude and phase corrections
		observation management
		web-based dashboard

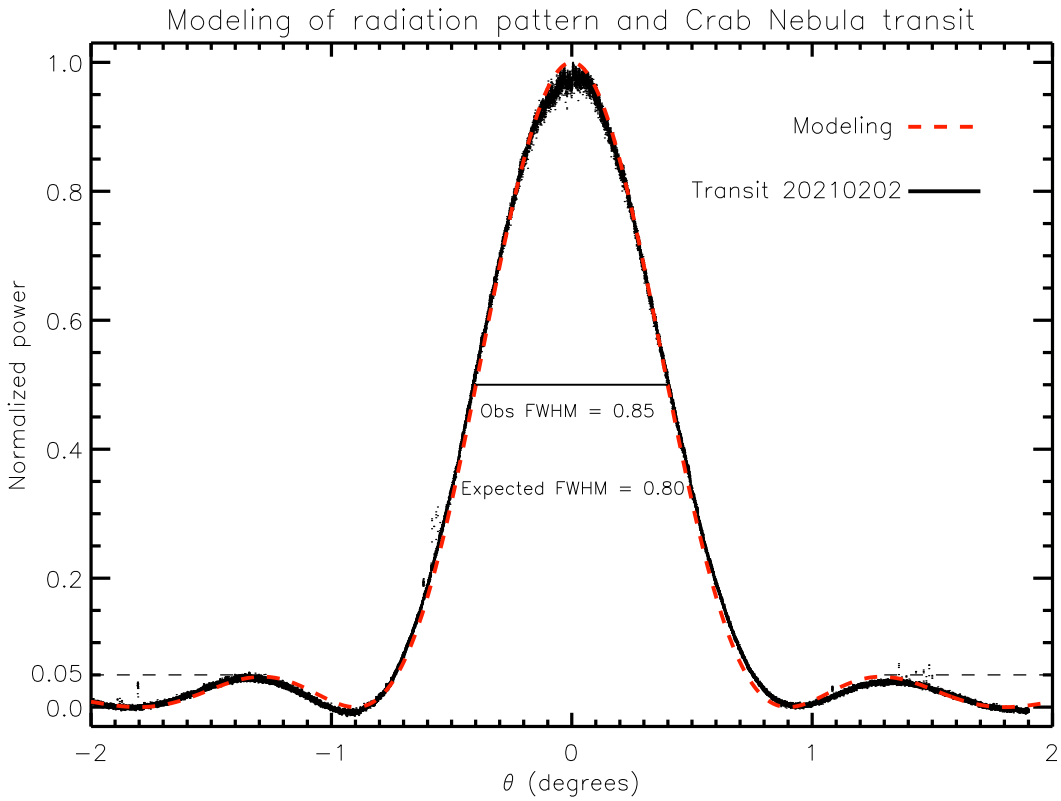

Figure S5. Digital system. Comparison (overlapping plots) between the theoretical beam pattern (red curve) and the measurement of the transit of a calibration source (3C144) (black curve). The two values of Full Width at Half Maximum (theoretical and observational) show an excellent agreement. The MEXART's E-W beam pattern in total power mode performs as expected.

Table S2. Estimation of the minimum flux detected by MEXART's digital back-end and the system temperature for different bandwidths.

$\Delta\nu$	ΔS_{min} (Jy)	T_s (K)	ΔT (K)
24.4 KHz	23.45	891	57.0
2 MHz	3.55	1222	8.6
12.5 MHz	2.28	1962	5.5

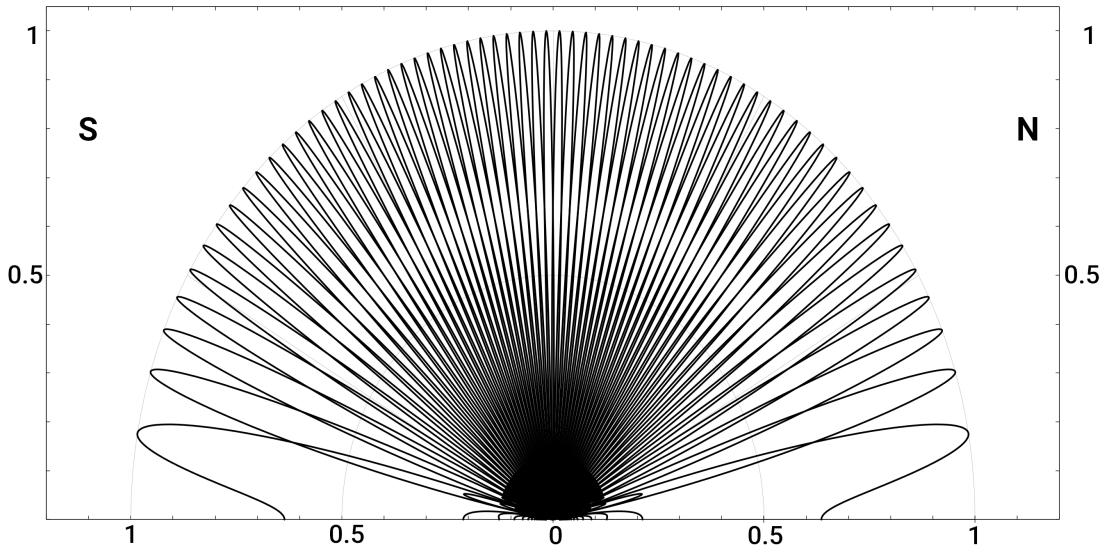

Figure S6. Digital system. Configuration of 62 fixed latitudinal beams at different declinations. Normalized electric far-field amplitude. The total angular coverage in the meridian is $\pm 72.4°$ respecto to the zenith. The beam pattern follows $\pm\, sin(\delta) = (n - 1/2)\,/\,32$, where n is the beam number (from 1 to 31) and δ is the angle between the local zenith and the beam direction.

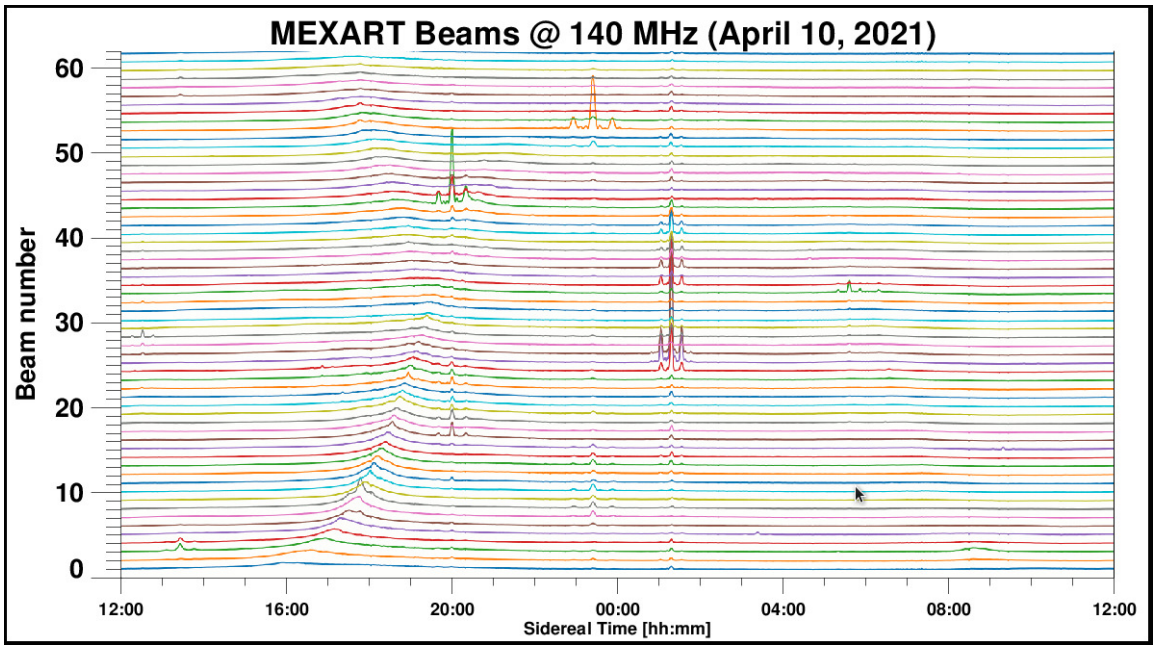

Figure S7. Integrated flux measurements of the 62 latitudinal beams indicating the transit of the Galaxy on April 10, 2021. The horizontal axis is sideral time (h:m), and the vertical axis is the integrated fluxes detected by the 62 latitudinal beams at different declinations (beam number).

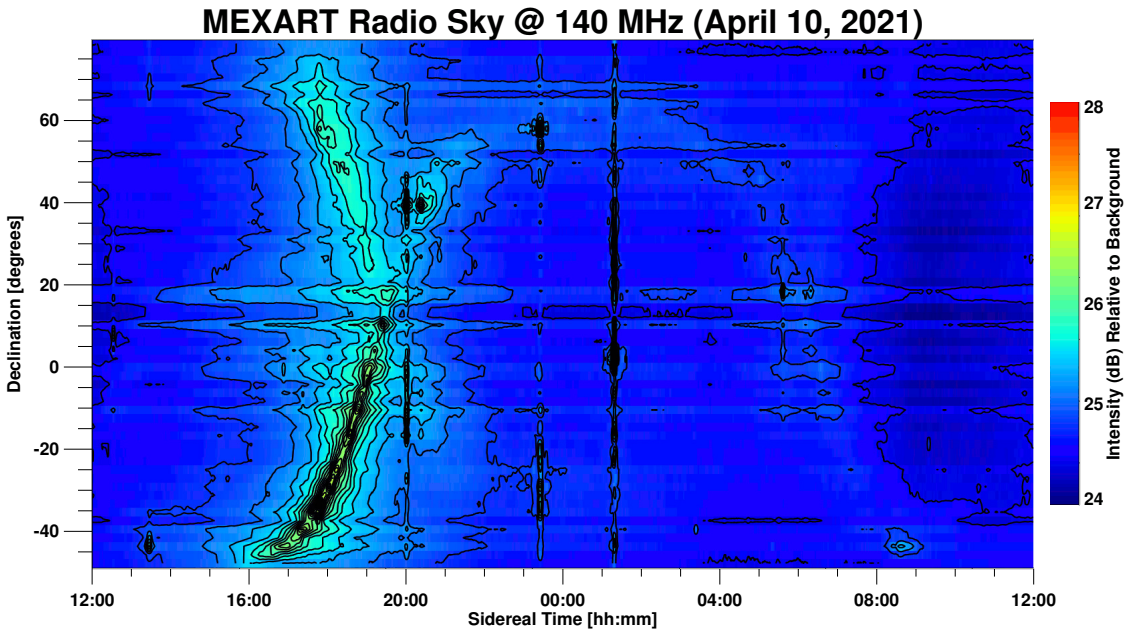

Figure S8. Transit of the Galaxy detected by MEXART at 140 MHz on April 10, 2021. The horizontal axis is sideral time (h:m), and the vertical axis is the radiation flux observation with 62 fixed latitudinal beams at different declinations (degrees).

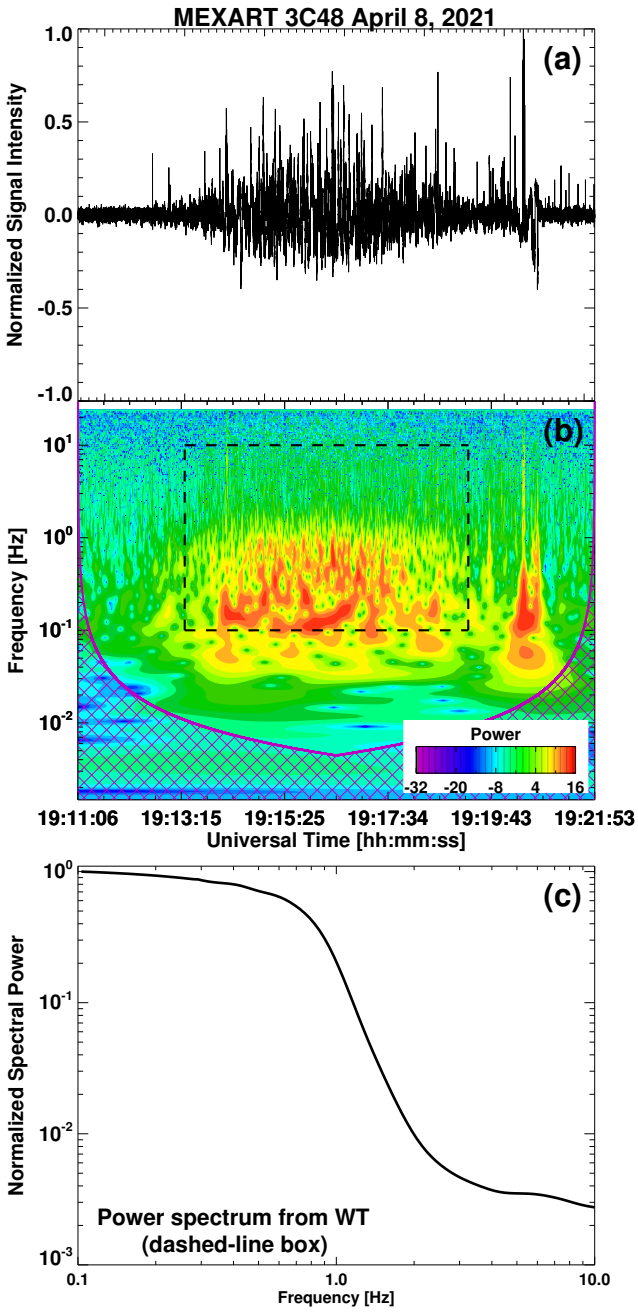

Figure S9. Measurement of the transit of an IPS radio source detected by MEXART on April 8, 2021, and data analysis to infer solar wind values. (a) Time series of the radio source 3C48 observed by MEXART on April 8, 2021. (b) wavelet (WT) applied to the time series, which allows us to identify regions where IPS is present. (c) Power spectrum of 3C48 at 140 MHz obtained from the dashed-line box in the WT power spectrum.

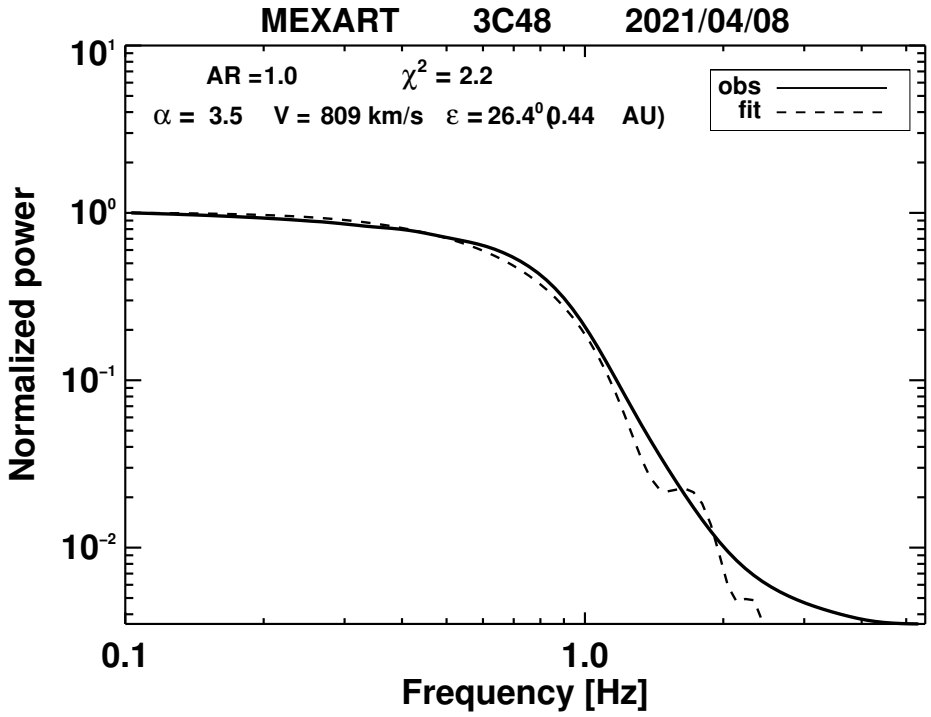

Figure S10. Single-station solar wind speed analysis for the observation of 3C48 on April 8, 2021. The single-station model fitting obtains a solar wind speed of 809 km/s.

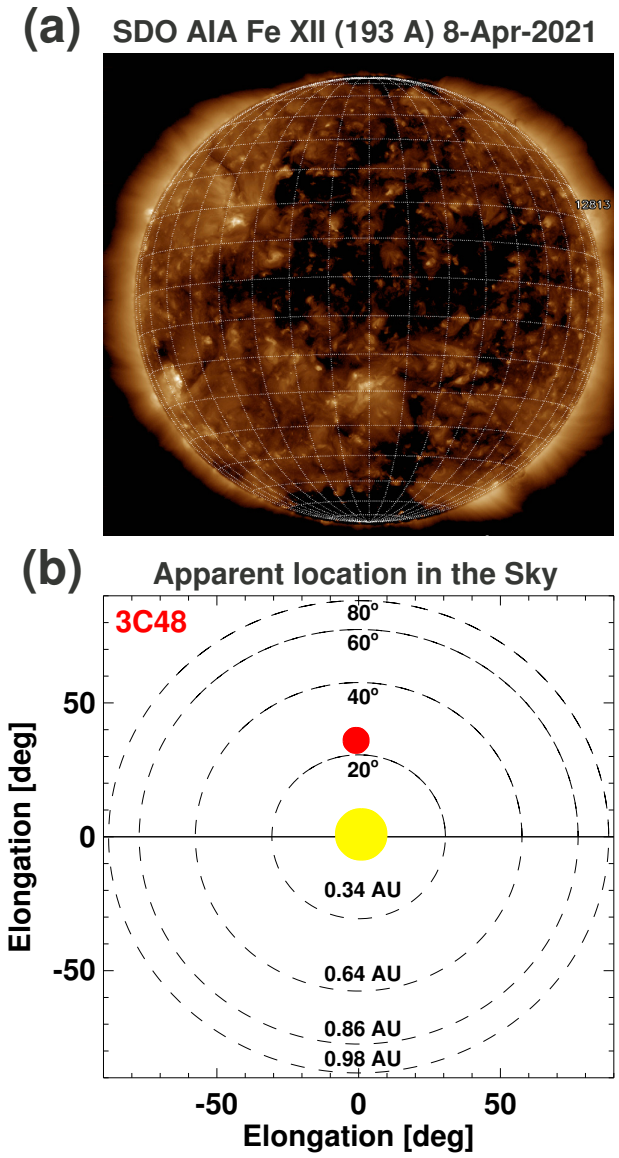

Figure S11. (a) the Sun observed on April 8, 2021, by the Atmospheric Imaging Assembly (AIA) onboard the Solar Dynamics Observatory (SDO) mission. (b) Relative position of 3C48 (red point) with respect to the Sun. The Earth's direction is perpendicular to the plane. The LOS of the radio source was crossing the region covered by a fast solar wind stream from the northern coronal hole.